MRS Advances (2026) 11:925–939
https://doi.org/10.1557/s43580-025-01393-7

REVIEW

A snapshot review on utilizing radiolysis in electrochemical liquid phase electron microscopy for accelerated degradation analyses

A. Lucía Morales[1,2] · Andreas Körner[1,2] · Birk Fritsch[1] · Giuseppe De Salvo[3] · Karl J. J. Mayrhofer[1,2] · Serhiy Cherevko[1] · Andreas Hutzler[1]

Received: 30 June 2025 / Accepted: 10 September 2025 / Published online: 19 September 2025

Abstract

Live imaging of electrochemical processes using electrochemical liquid phase electron microscopy (EC-LP-EM) setups is a cutting-edge research field, enabling insights into the dynamic behavior of the electrode–electrolyte interface at the nanoscale. Yet, size constraints in EC-LP-EM chips used for analyses add significant complexity, considering electrode architectures, mass transport properties, and operation. Additionally, radiolysis induced by electron probe–electrolyte interactions interferes with electrochemical signals. This snapshot review summarizes fundamental electrochemical concepts and how experimental observations are affected by the introduced radiolysis. Furthermore, we highlight studies that handled beam effects, obtaining *in situ* electrochemical data consistent with non-irradiated or *ex situ* counterparts. Instead of discussing artifacts, we propose ways for harnessing radiolysis to tailor harsher environments for accelerated stress tests (AST) to study degradation mechanisms of energy materials. This might aid particularly in the understanding and development of improved materials for electrochemical energy conversion devices, i.e., batteries, fuel cells, and electrolyzers.

Introduction

The research on sustainable energy materials and devices is driven by targets to reduce anthropogenic pollution, while still providing a reliable and affordable energy supply [1, 2]. In this context, electrochemical energy conversion and storage, e.g., utilizing batteries, fuel cells, or electrolyzers, has become increasingly important over the last decades, to expand the potential of renewable electrical energy from wind and solar. Particularly, the lifetime of these devices and their components is a crucial cost factor, and materials that can withstand the often harsh, dynamic reactor conditions are highly sought-after. Understanding the dynamic processes these materials undergo during operation is crucial to predicting their behavior in the long run and designing more efficient devices.

In situ and *operando* techniques such as electrochemical liquid phase electron microscopy (EC-LP-EM) and X-ray spectroscopy are powerful tools allowing us to comprehend electrochemical reactions and degradation mechanisms online. They have significantly advanced over the last decades, as reviewed elsewhere [2, 3]. Nonetheless, both expose samples to ionizing radiation during data acquisition, which inherently triggers radiation chemistry arising from the interaction between the irradiation sources with the electrolyte (solvent). [4–7] Acknowledging the impact of radiolysis is becoming relevant and discussed to acquire reliable electrochemical data [8–10]. Conventional electrochemical techniques provide a basic understanding of thermodynamics and kinetics of reactions at electrode interfaces. Moreover, for energy conversion reactions, they can provide information on the beginning of life (BoL), the transient, and the end of life (EoL) performance of electrocatalysts and other electrode materials. Electrochemical flow cells with on-line inductively coupled plasma mass spectrometry offer insights into the dissolution of materials during electrochemical bias [11, 12], but lack spatial resolution. Alternatively, identical

✉ A. Lucía Morales
l.morales@fz-juelich.de

✉ Andreas Hutzler
a.hutzler@fz-juelich.de

1 Forschungszentrum Jülich GmbH, Helmholtz Institute Erlangen-Nürnberg for Renewable Energy (IET-2), Cauerstr. 1, 91058 Erlangen, Germany

2 Department of Chemical and Biological Engineering, Friedrich-Alexander-Universität Erlangen-Nürnberg, Immerwahrstr. 2a, 91058 Erlangen, Germany

3 Nantes Université, CNRS, Institut des Matériaux de Nantes Jean Rouxel, IMN, 44000 Nantes, France

location transmission electron microscopy (IL-TEM) [13, 14], although capturing atomic resolution of intermediate states, lacks sufficient temporal resolution. Here, EC-LP-EM stands out due to its unmatched spatio-temporal resolution.

Several challenges of LP-EM have been summarized over the years [15, 16]. Some studies have focused on understanding radiolysis on LP-EM via radiation chemistry simulations [17, 18], while others have focused on mass transport properties and design of these nanoscale reactors [19, 20]. Furthermore, state-of-the-art reviews in the field, having a materials perspective, covered workflows for batteries [21], and electrocatalytic materials [22]. All these efforts have aided in the understanding of electrochemical reactions *in situ*, while acknowledging the need to mitigate beam effects to avoid artefacts.

However, in this perspective, we seek to complement those reviews by providing an electrochemical view on the implications and opportunities of utilizing radiolysis in EC-LP-EM. By proposing the use of the default radiolysis effects in EC-LP-EM experiments for accelerated stress test studies *in situ*, we highlight new methodological possibilities aiming to understand degradation mechanisms to enhance future technologies.

Radiolysis in EC-LP-EM

EC-LP-EM offers the ability to perform live imaging and understand electrochemical processes at interfaces at open circuit potential (OCP), when no current flows through the external circuit, or under bias supply (potential or current) conditions. Experiments are usually conducted in electrochemical cells (EC-cells) with three electrodes immersed in an electrolyte. In three-electrode setups, a reference electrode (RE) is used to determine the absolute potential applied to the working electrode (WE) while current is always transmitted and measured between the WE and counter electrode (CE), controlled through a potentiostat.

EC-cells are designed to encapsulate liquid and have electron-transparent windows that allow the trajectory of an electron probe through the electrochemical reactor compartment. The imaging signal features structural changes on the electrode–electrolyte interfaces. Such observations are always accompanied by the unavoidable radiation chemistry induced by inelastic electron-liquid interactions. In (diluted) aqueous solutions, irradiation with an electron probe excites and ionizes water, generating a plethora of primary species (Eq. 1) which then trigger chemical reaction cascades [5, 6].

$$\mathrm{H_2O} \xrightarrow[radiation]{high-energy} \mathrm{H^+, OH^-, OH, H, HO_2, H_2O_2, H_2, e_h^-} \quad (1)$$

In the next sections, we break down how electrode architectures influence electrochemical responses and how radiolysis affects the stability of electrode potentials. We also point out ways to tailor redox and acid environments via radiolysis and highlight recent examples of EC-LP-EM studies achieving reliable electrochemistry.

Impact of electrode architecture

Typical electrochemical cells used for EC-LP-EM studies consist of two microfabricated chips, which feature electron-transparent windows, typically consisting of SiN_x. One of the chips can have an additional spacer layer, and the other one features thin, insulated electrode connections, leaving only the tip of the electrodes (WE, CE, RE) uncoated for bias supply. Some designs have the spacer also on the same chip as the electrodes. In essence, resembling bulk EC-cells, although 6 to 9 orders of magnitude smaller. Electrode designs differ in electrode configurations, dimensions, and materials used. Figure 1a shows different electrode architectures of EC-chips. Once assembled, they have several thousand μm^3 of volume [19, 23] that can be filled with liquid via a syringe pump or via a differential pressure microfluidic system, creating a thin exchangeable liquid layer in which electrochemistry can take place.

However, an ongoing challenge is how to place the electrodes, considering the limited space, to have a homogeneous response of the electrochemical signals. In bulk electrochemistry, the placement of the WE with respect to the RE and CE is important so that artifacts in the electrochemical signals collected by the potentiostat are avoided. The potential at the WE is applied considering the potential difference between the RE and WE. Thus, placing them closer minimizes ohmic resistances. Although contaminations coming from the RE are still possible in bulk electrochemistry, e.g., Cl^- leak from Ag/AgCl in KCl electrolytes [24]. Furthermore, proximity might be a matter of dimensions. As proof of concept, by connecting an external bulk standardized RE connection to the EC-LP-EM (Fig. 1b), the cycling of a reversible iron redox couple was successfully controlled *in situ* [25]. Alternatively, one system features a miniaturized Ag/AgCl RE at the tip of the holder [26].

In contrast, the current is measured between the WE and CE. Redox reactions occur simultaneously due to charge balance; hence, charge-compensating reactions will happen at the CE. To ensure that the measured current is limited by the processes on the WE only, the CE must have a sufficiently large surface area so that the current is not restricted by its reactions. Furthermore, for bulk electrochemistry, modeling indicated that the best way to achieve homogeneous electric fields between WE and CE is when they face each other [27–29].

Simulations of electrode architectures (Fig. 1c) outline the impact of the CE position on the WE. Certain WE areas

are more prone to enhanced electrochemical response due to the inhomogeneities in the electric field profiles formed. In the case of a parallel configuration architecture, an increased electric field density is especially seen at the tip of the WE and at the sides that face the CE [30, 31]. For the concentric CE design case, the highest electric field density is concentrated at the tip [3, 31]. Furthermore, the height limitation has also proven to influence the electrochemical responses [30].

Due to these inhomogeneities in the current density distribution, even if the whole WE is visible in the window area, it is important to mention the specific WE location at which the imaging data were collected to visually compare WE areas not imaged, as suggested in literature [3]. Furthermore, the EC-LP-EM community could benefit from showing their results by means of current density, as done in bulk electrochemistry, aiming to compare results between *in situ* studies.

The choice of materials acting as WEs is another important factor in electrode architecture. The reasons are that WEs can undermine the image contrast of the processes of interest, form galvanic couples between WE and the material studied, or due to their catalytic activities that can drive parasitic reactions during data acquisition. Typical materials used are Au, Pt, glassy carbon (GC), TiN_x, or graphene on Pt. While Pt or Au WEs are clearly visible in the viewing window, GC and TiN_x WEs allow observation of processes on top of the electrode with resolutions comparable to regions next to the electrode, due to lower material contrast. The case of the formation of intrinsic built-in potentials at the WE was evident in a graphene-coated Pt WE, where electrodeposited Cu dissolved immediately after the reductive hold stop [33].

Lastly, the effects of strong (and possibly changing) electrical and magnetic fields, to which the EC-cell is exposed in the microscope, have not yet been addressed. Insulating materials such as SiN_x windows charge up under irradiation via secondary electron emission, leaving a positively charged surface. This window charging effect was experimentally shown to trigger water condensation, attributed to shifts of vapor–liquid equilibrium upon electric field exposure [34]. Furthermore, in bulk electrochemistry, electrostatic charges have driven redox reactions without a bias supply [35]. Note the height restriction in *in situ* EC-cells.

Moreover, all electrochemical cells used in EC-LP-EM experiments are exposed to the presence of magnetic fields of the objective lens of the microscope. In bulk electrochemistry, researchers have shown an increase in the electrochemical performance of Ni, Co, and Rh-based catalysts on the oxygen evolution reaction (OER) [36–39], and others on the oxygen reduction reaction (ORR) [37] in the presence of a magnetic field. These studies attribute this improvement to better mass transport of ions and of bubble release at the electrode surface. Others attribute these enhancements of electrocatalytic activity to the spin orientation of electrons under reaction conditions. This shows the influences of magnetism on electrochemistry being still poorly understood [40].

Electrode potential instabilities triggered by radiolysis

Electrochemical reactions comprise electron-transfer reactions via redox couples, generalized in Eq. 2 [41]. An oxidized species (Ox) gaining a stoichiometric number (n) of electrons (e^-) is in equilibrium with its reduced state (Red) and balanced with their respective stoichiometric coefficients (ν).

$$\nu_{Ox} Ox + n e^- \rightleftharpoons \nu_{Red} Red \tag{2}$$

In solid materials such as electrodes, electron transport proceeds along conductive pathways. The oxidized and reduced species are transported through a medium called electrolyte (liquid or solid). The electron probe, either in scanning (SEM), scanning transmission (STEM), or TEM mode, can interact with the electrolyte, opening radiolytic chemical reaction pathways upon imaging (Eq. 1) and thus generating new concentration gradients which may differ from conditions without irradiation (Fig. 2a). This can change the experimental conditions during data acquisition and thus influence electrochemical signals. The chemical shift due to radiolytic reactions can be calculated as formal electrode potentials of inorganic radicals [42]. Furthermore, these radiolytic reactions vary between EM operation modes (TEM vs. STEM vs. SEM) [43] and mass transport mechanisms (diffusion vs. convection) within the imaged volume [20].

Formal potentials in electrochemistry are calculated using the Nernst equation (Eq. 3).

$$E = E^0 + \frac{RT}{nF} \ln\left(\frac{C_{Ox}}{C_{Red}}\right) \tag{3}$$

The formal potential (E) of a redox couple considers its standard potential (E^0) calculated at standard conditions (25 °C, 1 atm, and 1 M concentration of reactants), in addition to temperature (T) and the ratio between the oxidized and reduced species concentration (C), with (R) and (F), as gas and Faraday constant, respectively [41, 44, 45]. When more than one redox couple is acting at the electrode interface, the potential evolves into a mixed potential, where, under equilibrium conditions, cathodic and anodic currents from different redox couples are equal, resulting in a net-zero current response [46].

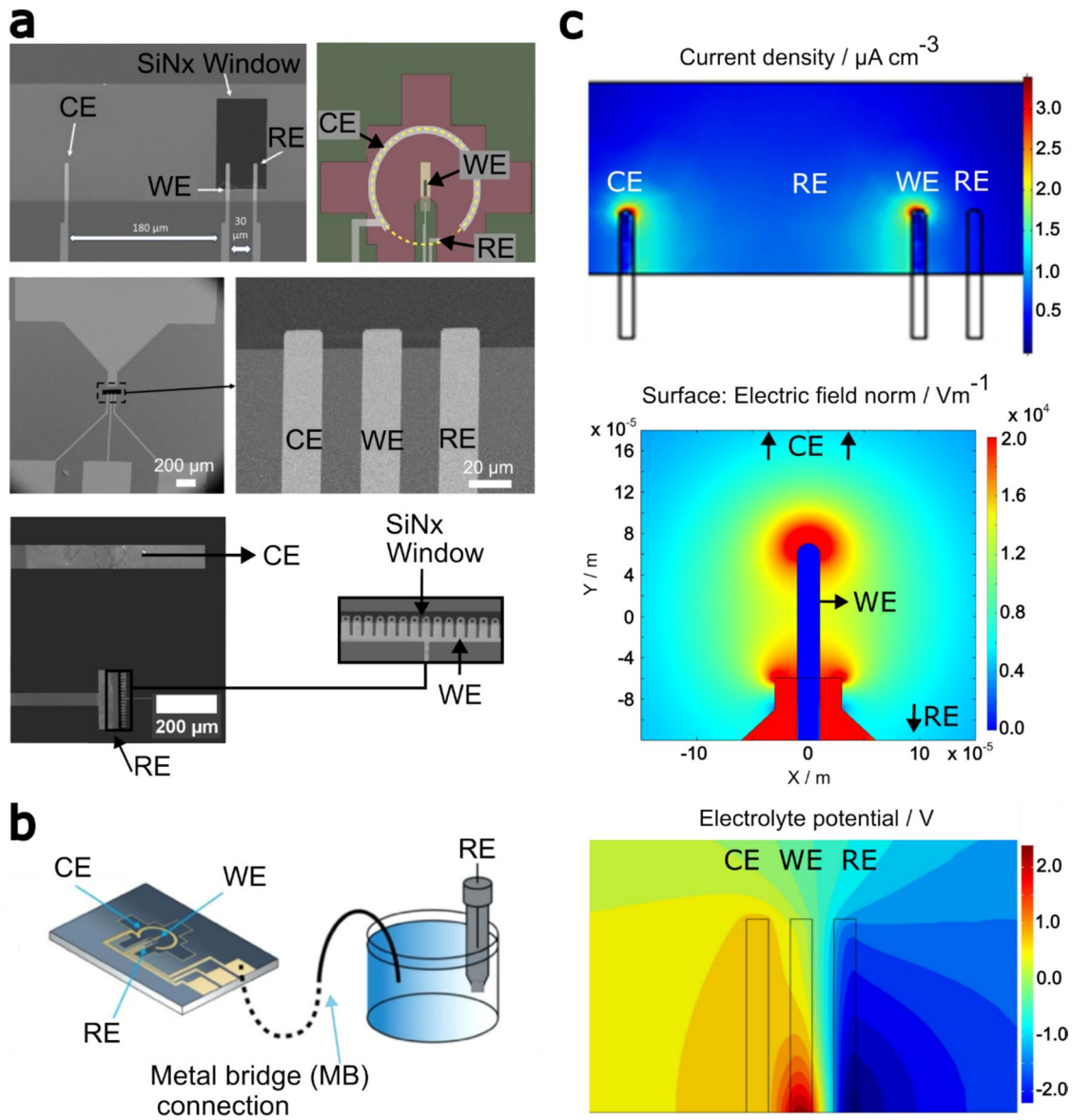

Fig. 1 Electrochemical cells are available for performing EC-LP-EM experiments *in situ*. The different electrochemical chip designs allow three-electrode connections to a potentiostat for electrochemical control. **a** Four different electrode architectures from EC chips for *in situ* EC-LP-EM experiments. The designs include electrodes with parallel alignments. Reproduced from Ref. [30], © 2024 The Author(s) under CC BY 4.0 license; and reproduced from Ref. [31], copyright © 2024, The Author(s). Published by Elsevier Inc. under CC BY 4.0 license. With concentric designs between the WE and CE. Adapted with permission from Ref. [32], copyright © 2025, American Chemical Society. Designs also offer WEs consisting of several smaller fingers, with the CE aligned diagonally to the WE. **b** Electrode architecture consisting of an EC-cell chip coupled to an external reservoir containing an established bulk RE. The two electrochemical cells are connected via a metal 'bridge' connection. Reproduced from Ref. [25], copyright © 2022 The Author(s) under CC BY 4.0 license. **c** Electrode architectures with respective 2D or 3D finite element simulations of the current density, electric field, and electrolyte potential profiles. All showing the inhomogeneous distributions on the WE of the electrochemical response. Reproduced from Ref. [30], © 2024 The Author(s) under CC BY 4.0 license; according to Yang, Feijóo *et al.* [3]; and Ref. [31], copyright © 2024 The Author(s). Published by Elsevier Inc., under CC BY 4.0 license

In situ EC-LP-EM experiments with irradiated electrolytes are often far from ideal conditions. Firstly, the temperature term might fluctuate due to electron beam-induced heating of the specimens [47–50], which then might influence intrinsic properties of electrolytes, mass transport of species, as well as redox kinetics [41, 51]. This heating will be more pronounced at higher dose rates, lower acceleration voltages, and in surroundings of low thermal conductivity [19, 48, 50, 52]. Furthermore, the presence of parasitic radiolytic reactions will create a more complex mixed potential behavior

than a potential following Eq. 3, of only one redox couple at equilibrium. In EC-LP-EM experiments, all possible redox and radiolytic reactions at the WE need to be considered for interpreting the mixed potential and evolving processes.

Evolution of radiolytic products (Eq. 1) such as H_2 and O_2 concentrations during LP-SEM was monitored by measuring the OCP (depicted in Fig. 2b), using an EC-cell consisting of a Pt WE and CE, and a Ag/AgCl RE [53]. Disturbances in equilibrium concentrations of electrochemical reactions led to a shift in the mixed potential compared to bulk electrochemistry with Ar-purged electrolytes. Moreover, imaging only parts of the WE minimizes the impact of radiolysis on the total electrochemical signal since less electrolyte volume is irradiated. Thus, discrepancies between what we observe at the viewing window compared to other WE locations not imaged are expected. Such inhomogeneous behavior is important to handle with care during data analysis.

pH is an important variable in electrochemistry, which influences the potential at which redox reactions can occur, considering the experimental conditions, i.e., specific electrolyte concentrations. In LP-EM, under certain experimental conditions, the concept of pH can break down upon irradiation with more than 10^3 Gy/s of dose rates (the total energy absorbed by matter in units of Gray per second) as a consequence of the radiolytic generation of H^+ and OH^- (Eq. 1) as depicted in Fig. 2a. These species will be consumed unevenly, decoupling their concentration ratio depending on the individual radiolytic reaction networks of the electrolytes (additives) used [54]. Hydrogen evolution and oxidation reactions (HER/HOR), Eq. 4, are an example of a redox couple that involves H^+. They, like other electrochemical reactions, can be depicted with Pourbaix diagrams, hinting at the electrochemical behavior of inorganic species depending on potential and pH (Fig. 2c) [55, 56].

$$2H^+ + 2e^- \rightleftharpoons H_2 \qquad E^\circ = 0.00\ \text{V}\ \textit{vs.}\ \text{SHE} \tag{4}$$

The standard potential of the hydrogen redox couple is 0 V at 0 pH (turquoise point in Fig. 2c). This point is the reference of the standard hydrogen electrode (SHE) scale, assuming standard conditions. Because acidity shifts in EC-LP-EM are possible due to radiolysis, experimental data might deviate from standardized scales. Since many reactions depend on pH in a similar manner, it is convenient to present them in the reverse hydrogen electrode (RHE) scale, making them pH-independent (new zero reference potential, red line in Fig. 2c). Simulations of the acidity of LiCl, LiBr, and $LiNO_3$ (1 and 10 mM) solutions irradiated by electrons and X-rays (Fig. 2d) have also illustrated the change in acidity during observation. Due to the different reaction networks of each electrolyte, the results indicated distinct radiolytic acidity $\left(\pi^* = \log\left(\frac{c(H^+)}{c(OH^-)}\right)\right)$ for the both cases [54].

In bulk electrochemistry, the use of concentrated electrolytes and buffer solutions is recommended. This minimizes pH fluctuations and secures good ionic conductivity so that electrodes are sufficiently screened and processes are diffusion-dominated [41]. However, in EC-LP-EM, non-diluted electrolytes can no longer neglect solute radiolysis [6, 54, 57]. Similarly, radiolysis of buffers creates more radiolytic side products with case-dependent consequences. These effects may shift electrochemical behavior, or presumably, parasitically interact with the materials of interest. Accounting for deviations in the acidity and chemistry of electrolytes attributed to radiolysis is fundamental for achieving quantitative electrochemistry in EC-LP-EM and synchrotron experiments. For example, by coupling these extra reactions, when possible, to the reaction sets used for Pourbaix diagrams construction.

Instabilities can further be caused by poor potentiostat grounding during EC-LP-EM experiments or incorrect use of reference electrodes. Pseudo-REs (pREs) consisting of Au, Pt, or GC are polarizable and do not offer stable reference potentials. Pt, furthermore, is the benchmark catalyst for ORR, and it has a limited activity towards OER [56, 58]. Its reference potential consists of a mixed potential of all possible reactions (Fig. 2c, Pt Pourbaix diagram) at its interface: platinum dissolution (Eq. 5), passivation (Eq. 6), ORR/OER (Eq. 7).

$$Pt^{2+} + 2e^- \rightleftharpoons Pt \qquad E^\circ = 1.00\ \text{V}\ \textit{vs.}\ \text{SHE} \tag{5}$$

$$PtO + 2H^+ + 2e^- \rightleftharpoons Pt + H_2O \qquad E^\circ = 1.19\ \text{V}\ \textit{vs.}\ \text{SHE} \tag{6}$$

$$O_2 + 4H^+ + 4e^- \leftrightharpoons 2H_2O \qquad E^\circ = 1.23\ \text{V}\ \textit{vs.}\ \text{SHE} \tag{7}$$

Hence, its potential can shift during experiments. Consequently, the potential difference between the reference and the working electrode of interest is often artificially fluctuating, which can be easily overlooked in data evaluation. The electrochemistry of Pt exemplifies how diverse responses from cyclic voltammetry profiles can look depending on the experimental pH, affecting onset potentials of reactions (Eq. 4 and Eq. 7), interactions of species in the electrolytes towards Pt, or even its crystallography [59–63].

An alternative approach uses a miniaturized Ag/AgCl RE in the holder. Still, when measuring potentials of a same redox couple with a Ag/AgCl RE in bulk vs. *in situ* experiments, a 0.4 V shift was observed between the electrochemical signals of interest [26]. Proper RE calibrations between *in situ* with *ex situ* setups that replicate the electrochemical reactions of interest can give certainty that the redox behavior of the material is neither under- nor overestimated due to potential instability [26, 64–66].

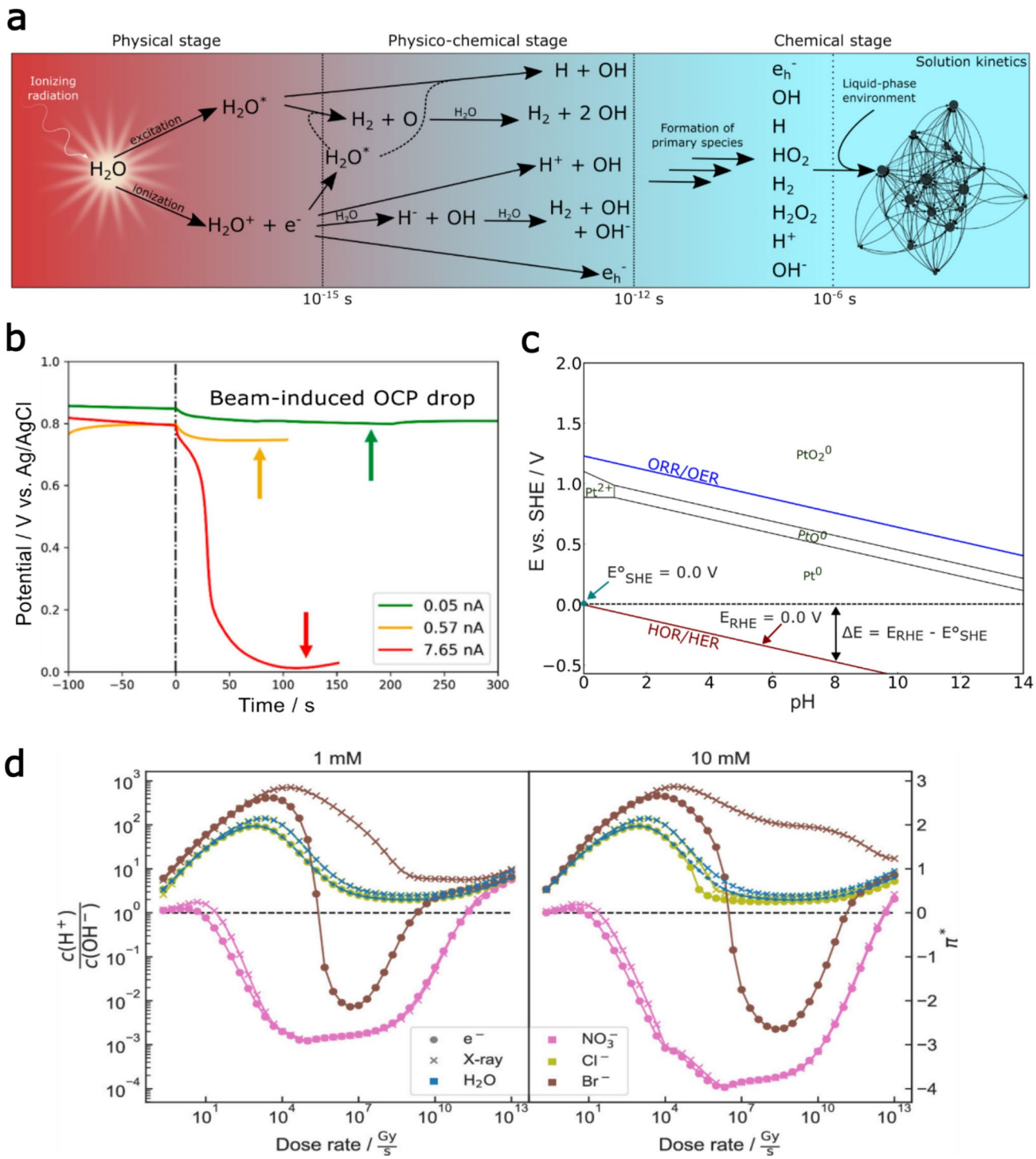

Tailoring redox environments utilizing radiolysis

Since the infancy of LP-EM, observations have shown the ability to tailor chemistry to drive the growth and dissolution of electrocatalysts *in situ*. However, the fundamentals causing these events were not clear enough to be applied in a controlled manner [67]. Several studies used beam-induced reductive species to initiate nanoparticle growth, and study new growth mechanisms [18, 68, 69]. It was also possible to obtain insights into the dissolution mechanisms of grown nanoparticles by oxidative radiolysis products. Figure 3a exemplifies this for Au etched by $ClOH^-$, an oxidative species formed via radiolysis of the chloride-containing precursor solution [18, 70, 71]. Other studies captured galvanic replacement reaction events, showing how less noble metal

◂**Fig. 2** Radiolysis shifts the parameter space of possible electrochemical reactions. **a** Electron-water interactions create primary species within µs. The radiolysis products then react via a complex reaction cascade. Reproduced from Ref. [54], copyright © 2023 The Authors. Published by American Chemical Society under CC BY 4.0 license. **b** Irradiation products induce a drop in open circuit potential (OCP), with the effect being more pronounced for higher beam currents in SEM. The drop in OCP is attributed to the identification of H_2 in contact with the Pt electrode surface, simulating a RHE RE. Reprinted with permission from Ref. [53], copyright © 2023, American Chemical Society. **c** Pourbaix diagrams provide information about the possible stable phases of inorganic species at a given potential and acidity. Here, Pt as a common electrode material in EC-LP-EM systems is displayed in addition to the HER/HOR and ORR/OER equilibrium reactions, which can occur at the surface of Pt. The HER/HOR redox couple at standard conditions is used as the reference point for standard electrode potentials of redox couples, defining 0 V. In the Pourbaix diagram, the turquoise point depicts the reference point of the standard hydrogen electrode (SHE) scale. In contrast, the red line, which describes the hydrogen redox couple equilibrium, following the Nernst equation (Eq. 3), represents the reverse hydrogen electrode (RHE) scale. This scale sets the zero value across all pH values, allowing electrochemical potentials to be reported at a scale independent of pH. Adapted with permission from Ref. [45], copyright © 2020, American Chemical Society. Adaptation created using Pourpy python package from Ref. [55] and data from Ref. [56]. **d** Simulations using G-values of electrons and X-rays indicate that the radiolytic steady state concentrations of H^+ and OH^- decouple. This depends on additives (electrolytes), e.g., LiCl, LiBr, and $LiNO_3$. The left panel shows the results for 1 mM solutions, whereas the right panel shows the results for 10 mM. The dotted line corresponds to a neutral state $\left(\frac{c(H^+)}{c(OH^-)} = 1\right)$. As the pH-value alone does not suffice to describe the acidity of the solution, the radiolytic acidity $\left(\pi^* = \log\left(\frac{c(H^+)}{c(OH^-)}\right)\right)$ is introduced. Reproduced from Ref. [54], copyright © 2023 The Authors. Published by American Chemical Society under CC BY 4.0 license

nanoparticles act as sacrificial templates to allow the reduction of more noble metal precursors (Fig. 3b). For the cases using bimetallic nanoparticles, their galvanic connection caused preferred dissolution events of the less noble metal due to their higher tendency to oxidation [72–77]. These results show different dissolution rates and mechanisms depending on the intrinsic stability of facets, but were also largely influenced by the chemistry, and consequently radiation chemistry, of their precursor solutions, including solvents or already introducing scavenger species.

First radiation chemistry simulations helped in interpreting the trends observed in LP-EM results, and since then, they have become a complementary toolbox for experimental design [17]. Furthermore, simulations evolved to include much more complex radiation reaction networks of inorganic and organic solutions beyond water [78, 79]. For instance, in the attempt to control the formation of these radiolytic species, the LP-EM community adopted the concept of adding scavenging agents in experiments [72, 74] that showed to mitigate the effect of radicals on the materials studied. However, deeper studies, including simulation results, allowed for the investigation of more scavenging species at once and identified that they can be effective depending on the scenario [80]. Thus, showing the ability to scavenge certain radiolytic species, but in turn, introducing new reaction cascades. Alternatively, "redox buffering" for radiolysis can be applied, adjacent to conventional pH buffering, by adding solutions containing redox couples of V, Cr, or Ce, among others. The targeted potential control is achieved through the formal electrode potential of their inorganic radicals formed. By focusing on oxidative potentials relevant in electrochemistry, they successfully evaluated degradation mechanisms of various electrocatalysts (Fig. 3c) [81, 82]. This method was recently applied to yield specific suggestions for IrO_2 electrocatalyst design to achieve good activity and stability towards OER, simultaneously [83].

Control over the redox environment can also be achieved by varying solution flow rates and dwell times in LP-STEM experiments. Typical STEM dwell times are insufficient to reach a radiolytic steady state: initially, primary products (see Eq. 1) are formed. Secondary products, such as O_2, are produced in the following reaction cascade (Fig. 3d). This subsequent build-up of secondary products allows for altering the (electro)chemical environment via STEM dwell time. Likewise, mass transport (e.g., steep diffusion gradients or liquid flow) affects the build-up of secondary species [19, 20]. Short-lived, primary products are formed too rapidly to be flushed away effectively [7]. For silver (Fig. 3d), oxidative environments are favored with low flow rates and long dwell times. In this scenario, radiation chemistry cascades allow for notable oxygen build-up, whereas reductive primary species (e_h^-, $H^\cdot$) dominate at high flow rates and short dwell times. With this, a transition between reductive and oxidative environments was successfully achieved, leading to growth and dissolution events depending on the set experimental parameters [23]. This proves the possibility of experimentally achieving a net-zero radiolytic state, through an equilibrium between the reductive and oxidative radiolytic species that compares to a non-irradiated equilibrium state by adjusting experimentally controllable parameters, as was suggested before [17]. Hence, the image quality does not necessarily need to be heavily sacrificed by means of a lower irradiation dose rate to mitigate unavoidable beam effects.

The studies in Fig. 3 did not employ a potentiostat to control the growth/dissolution of electrocatalysts. Nevertheless, these experiments studied electrochemical processes driven by solution composition changes at electrode/solution interfaces. Still, investigating electrochemical reactions in EC-LP-EM controlled via a potentiostat is important since electrochemical protocols such as cycling, ramps, holds, pulses, which are controlled through an external bias supply, provide further transient and kinetic information of electrochemical processes.

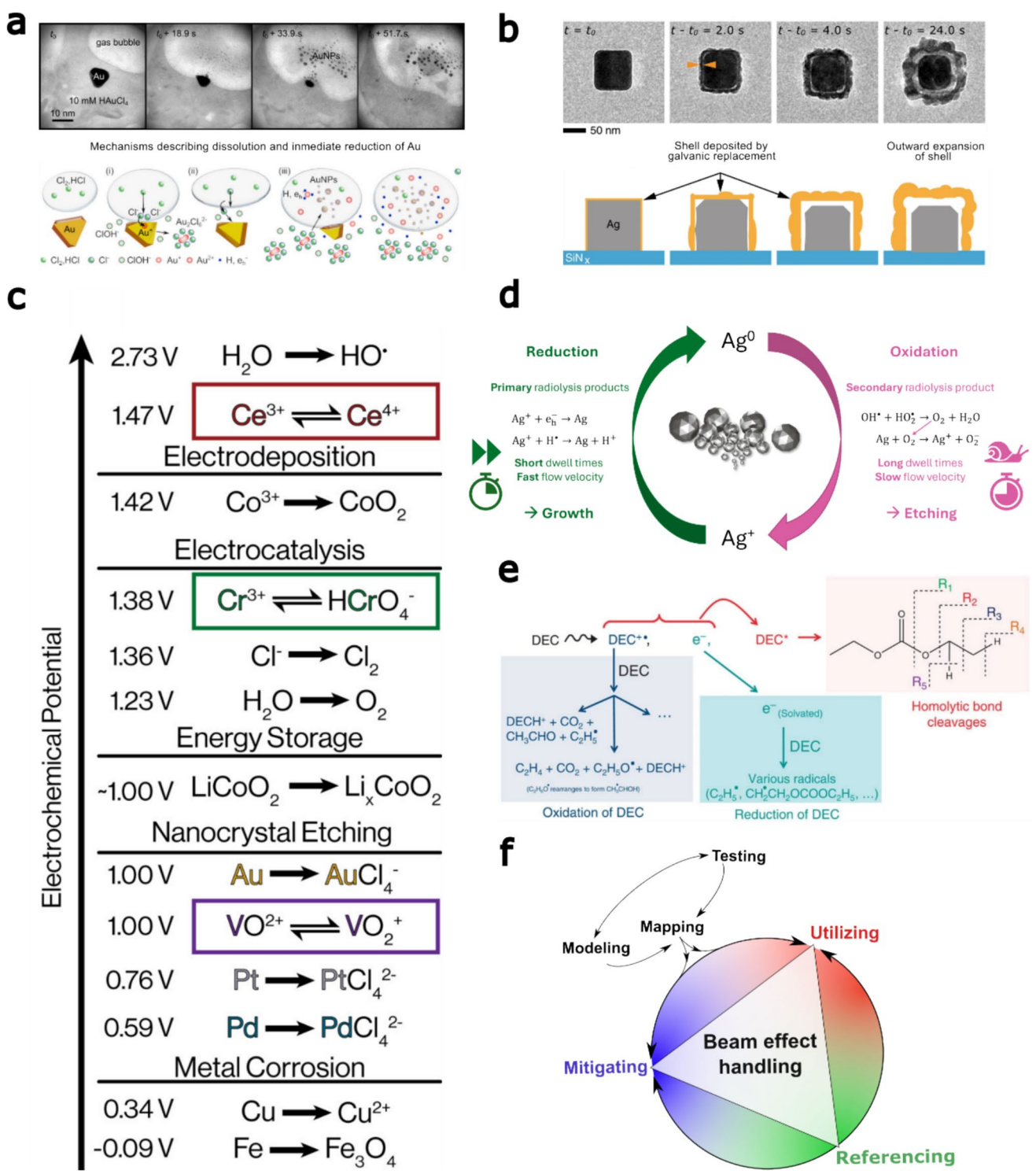
a
gas bubble
Au
10 mM HAuCl4
10 nm
AuNPs
Mechanisms describing dissolution and inmediate reduction of Au
b
t = t0
t - t0 = 2.0 s
t - t0 = 4.0 s
t - t0 = 24.0 s
50 nm
Shell deposited by galvanic replacement
Outward expansion of shell
Ag
SiNx
c
Electrochemical Potential
2.73 V H2O → HO•
1.47 V Ce3+ ⇌ Ce4+
Electrodeposition
1.42 V Co3+ → CoO2
Electrocatalysis
1.38 V Cr3+ ⇌ HCrO4-
1.36 V Cl- → Cl2
1.23 V H2O → O2
Energy Storage
-1.00 V LiCoO2 → LixCoO2
Nanocrystal Etching
1.00 V Au → AuCl4-
1.00 V VO2+ ⇌ VO2+
0.76 V Pt → PtCl42-
0.59 V Pd → PdCl42-
Metal Corrosion
0.34 V Cu → Cu2+
-0.09 V Fe → Fe3O4
d
Reduction
Primary radiolysis products
Ag+ + e- → Ag
Ag+ + H• → Ag + H+
Short dwell times
Fast flow velocity
→ Growth
Ag0
Ag+
Oxidation
Secondary radiolysis product
OH• + HO2• → O2 + H2O
Ag + O2 → Ag+ + O2-
Long dwell times
Slow flow velocity
→ Etching
e
DEC
DEC+•, e-,
DEC*
DEC
DECH+ + CO2 + CH3CHO + C2H5•
C2H4 + CO2 + C2H5O• + DECH+
Oxidation of DEC
e- (Solvated)
DEC
Various radicals
Reduction of DEC
R1 R2 R3 R4 R5
Homolytic bond cleavages
f
Testing
Mapping
Modeling
Utilizing
Beam effect handling
Mitigating
Referencing

◂**Fig. 3** Electrochemistry is governed by equilibrium processes of redox chemistry. Out of equilibrium, one side of the reaction dominates, inducing growth or dissolution of the species under study. The use of radiolysis to tailor redox environments in EC-LP-EM can aid the characterization of materials under electrochemical protocols. **a** A gold platelet is etched at a solid–liquid-gas interface, and Au nanoparticles reprecipitate. The etching process is attributed to chloride species, and the following growth is attributed to the immediate Au^{3+} supersaturation state. Reproduced from Ref. [71], copyright © 2019 The Authors. Published by WILEY–VCH Verlag GmbH & Co. KGaA, Weinheim under CC BY 4.0 license; and reproduced from Ref. [86], unmodified image citation under § 51 UrhG (German Copyright Law). **b** A gold precursor solution at room temperature started a galvanic replacement reaction on a silver cube. The Au was reduced at the edges of the Ag cube, starting to grow outwards, while the Ag dissolved, evolving into a smaller circular shape in comparison to its initial state. Reproduced from Ref. [75], copyright © 2017, The Author(s) under CC BY 4.0 license. **c** Electrochemical potential of different redox couples interacting with radical species derived by radiolysis, seeking a "redox buffer" for radiolysis. This shows the ability to study degradation mechanisms by controlling potentials of interest via the addition of appropriate additives to liquid solutions, which will evolve potentials of inorganic radicals. Reprinted with permission from Ref. [81], copyright © 2021, American Chemical Society. **d** Reductive and oxidative environments can be controlled by experimental parameters such as dwell time and flow rates to grow or reduce Ag platelets. The Ag radiation chemistry and its resulting redox environments depend on the formation of primary (reductive) or secondary (oxidative) products. Reproduced from Ref. [23], copyright © 2024 The Author(s). Published by Elsevier Ltd. under CC BY 4.0 license. **e** AST protocols using pulse radiolysis are suggested to study diethylcarbonate (DEC) electrolyte degradation. The degradation pathways from radiolysis can originate similarly to the ones obtained from oxidation or reduction of DEC. The advantage lies in the faster progression of electrolyte degradation. Reproduced from Ref. [85], copyright © 2015, The Author(s) under CC BY 4.0 license. **f** Workflows for LP-EM experimental design *in situ*, including experimental and theoretical approaches for better planning of experiments. Adapted from Ref. [8], copyright © 2025 The Author(s). Advanced Materials published by Wiley–VCH GmbH under CC BY 4.0 license

By default, in EC-LP-EM studies, observations, radiolysis, and electrochemistry cannot be disentangled experimentally, even under a net-zero beam effect, since that is an artifact of another equilibrium. Thus, by being intentionally on either side, we could achieve a more profound electrochemical understanding. At the reductive side, exploring growth kinetics or radical-mediated degradation processes, or on the oxidative side, to investigate dissolution. This presents an open opportunity to establish accelerated stress test (AST) protocols that are electrochemically controlled under harsher environmental conditions, which are radiolytically controlled. This thought was already proposed a decade ago for studying electrolyte degradation of batteries using radiolysis with *in situ* LP-EM [84] and pulse radiolysis [85] experiments, where the degradation products obtained resembled the ones obtained in bulk electrochemistry.

Figure 3e shows that depending on the radiation chemistry of the electrolyte, following oxidation or reductive reaction pathways lead to different degradation products, either found at the anode or cathode side. Thus, the time scale to obtain these degradation products was accelerated by radiation chemistry, independent of the irradiation source. Following this logic, the effect of ionomer (solid electrolyte) degradation caused by radicals on fuel cell technologies can be investigated with EC-LP-EM.

In a sense, we are proposing to look at radiolysis as a tool we can now understand and leverage according to our needs. Workflows like the one in Fig. 3f are advantageous for EC-LP-EM studies towards careful experimental design, handling beam effect based on mitigation, as well as utilization. Besides, protocols for carrying out space-dependent radiolysis simulations for the inclusion of EC-cell setups are now available [87].

Beam effect handling: towards quantitative electrochemistry

The studies reported in Fig. 4 summarize examples of electrochemical processes controlled with a potentiostat and effective beam effects handling, resulting in robust quantitative results. Although they investigated different electrochemical systems, all of them performed extra experiments aiming to identify beam effects by three major approaches:

1) Intentionally exposing the systems to extended periods under different irradiation conditions,
2) Comparing beam-on/ beam-off experiments *in situ*, or examining non-irradiated areas; and
3) Performing *ex situ* experiments using bulk electrochemical cells to compare electrochemical signals, spectra, and structural changes via *post-mortem* analyses. Here we highlight how these approaches proved beneficial, and which aspects still need to be carefully considered.

Beam effects can be mitigated by, e.g., reducing the electron dose rate, which is the energy deposited per time into the liquid [88]. This can be controlled through experimental parameters that can be read from the microscope interface. Recent works in the field keep reducing dose rate by lowering beam current (A/s) [53] or lowering the electron flux density ($e^{-}/(Å^2 s)$) [32, 64, 89]. Note that the dose rate (Gy/s) is not the same as electron flux density, as recently reviewed [90]. The acceleration voltage is another available parameter we can control. For typical acceleration voltages used in TEM and SEM, the inelastic scattering cross section increases with decreasing primary electron energy [88] and, thus, radiolysis products are generated more frequently [47, 48, 52, 88].

All studies in Fig. 4 reduced beam exposure to minimize impacts on electrochemical signals by running electrochemical protocols with a blanked beam and only recording images

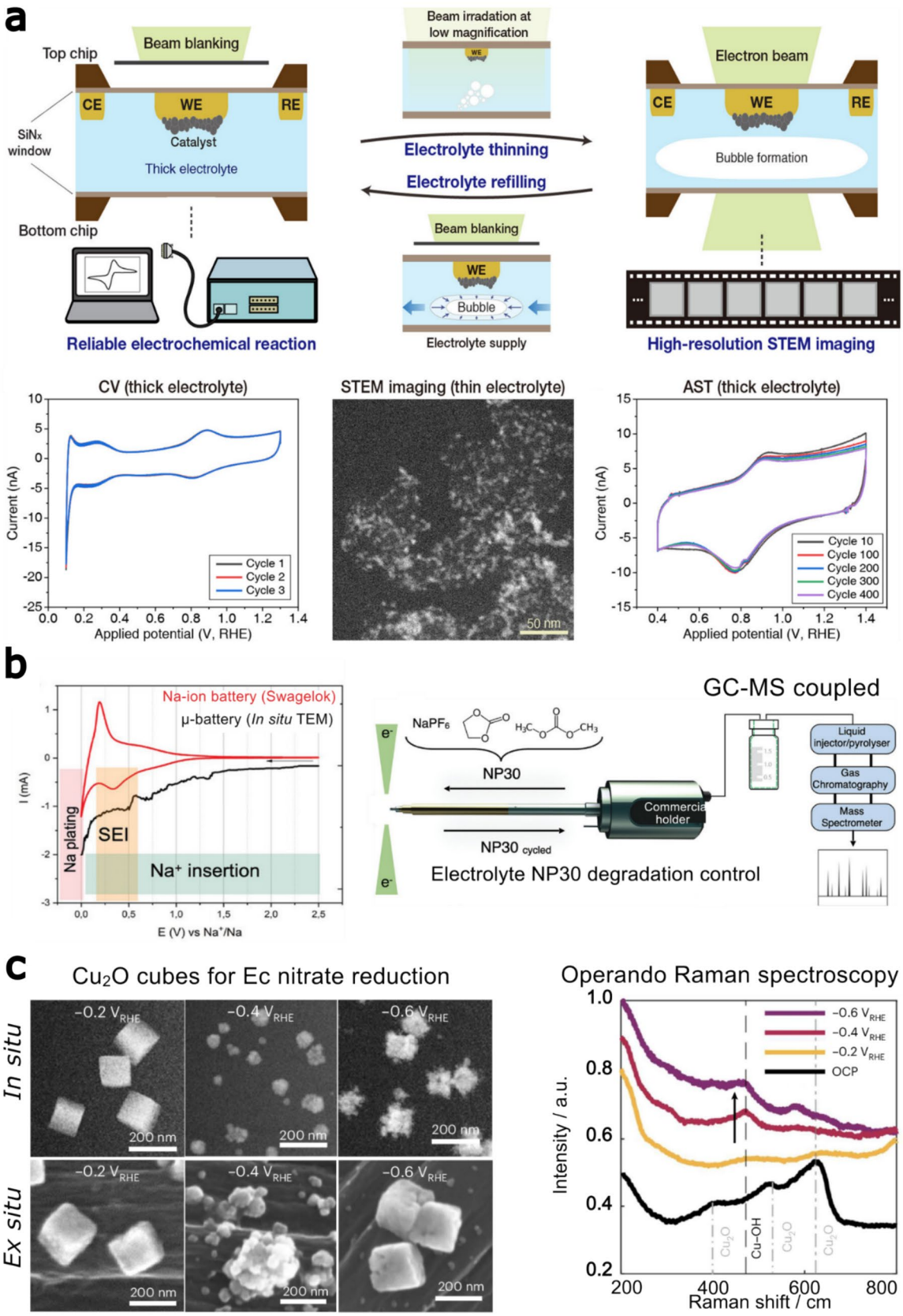
a
Top chip
Beam blanking
CE
WE
RE
SiNx window
Catalyst
Thick electrolyte
Bottom chip
Reliable electrochemical reaction
Beam irradation at low magnification
Electrolyte thinning
Electrolyte refilling
Beam blanking
Bubble
Electrolyte supply
Electron beam
Bubble formation
High-resolution STEM imaging
CV (thick electrolyte)
Current (nA)
Applied potential (V, RHE)
Cycle 1
Cycle 2
Cycle 3
STEM imaging (thin electrolyte)
50 nm
AST (thick electrolyte)
Cycle 10
Cycle 100
Cycle 200
Cycle 300
Cycle 400
b
Na-ion battery (Swagelok)
μ-battery (In situ TEM)
I (mA)
Na plating
SEI
Na+ insertion
E (V) vs Na+/Na
GC-MS coupled
NaPF6
NP30
NP30 cycled
Commercial holder
Liquid injector/pyrolyser
Gas Chromatography
Mass Spectrometer
Electrolyte NP30 degradation control
c
Cu2O cubes for Ec nitrate reduction
In situ
Ex situ
-0.2 VRHE
-0.4 VRHE
-0.6 VRHE
200 nm
Operando Raman spectroscopy
Intensity / a.u.
Raman shift / cm
OCP
Cu-OH
Cu2O

◂**Fig. 4** Towards quantitative electrochemical studies in situ EC-LP-EM. *In situ* electrochemical experiments must consider electron beam effects and propose strategies for their proper handling. *In situ* results could be verified by beam on/beam off experiments and with ex situ experiments. **a** Pt on carbon, a catalyst for fuel cell technologies, degrades under electrochemical cycling. The electrochemical and extended accelerated stress test (400 cycles) protocols are performed with a blanked beam and thick electrolyte conditions to reduce beam effects, whereas imaging is performed at thin electrolyte conditions achieved by the formation of electrochemical bubbles. Reprinted with permission from Ref. [32], copyright © 2025, American Chemical Society. **b** *In situ* Na-ion µ-battery study compared to *ex situ* experiments using a Swagelok cell setup. The study shows degradation products from the hexafluorophosphate (NP30) electrolyte in the *in situ* experiment by measuring the exhaust solution of the holder with a GC–MS instrument. Reproduced from Ref. [66], copyright © 2024 The Author(s). Small Methods published by Wiley–VCH GmbH under CC BY 4.0 license. **c** Cu_2O cubes degrade under electrochemical nitrate reduction reaction conditions. The study performed EC-LP-EM, synchrotron *operando*, and bulk *ex situ* electrochemical characterizations to corroborate results. The results from EC-LP-EM and synchrotron studies led to the same conclusions of degradation and reaction pathways under different reductive potential conditions. Still under harsh potential conditions, degradation of materials takes less time than under milder potentials in EC-LP-EM experiments. Reproduced from Ref. [64], copyright © 2025, The Author(s) under CC BY 4.0 license

of the previous and after states. Overall, they observed that the electrochemical signals, structural changes, or electrolyte degradation trends led to similar conclusions between beam-on/beam-off experiments. However, all concluded that beam effects cannot be ruled out completely. An *in situ* identical location (IL)-LP-EM strategy is useful for identifying beam effects. Still, the strength of using EC-LP-EM as a technique for recording the complete dynamic evolution of electrochemical reactions is lost with this approach.

Furthermore, bulk *ex situ* electrochemical experiments helped to gain an understanding of geometric effects introduced by microelectrode architectures. We consider that performing bulk electrochemical experiments alongside the *in situ* experiments increases the ability to grasp which electrochemical responses are expected and properly convert potentials of interest to the respective RE scales. By implementing these strategies, the observations in the experiments were attributed to electrochemistry rather than being driven by beam effects. This agrees with our suggestions that the beam effects are always entangled within overall reaction mechanisms and electrochemical data. Handling the beam effects of these *in situ* experiments was decided upon by imaging parameters where the least deviations between *in situ* and either *ex situ* or non-irradiated results were obtained, rather than parameters that completely mitigated beam effects. Furthermore, certain methodologies might still lead to beam effects.

EC-LP-EM studies achieve more stable electrochemical signals with increased liquid thicknesses, known in the EC-LP-EM community as thick electrolyte conditions [30, 91]. However, a drawback of enhanced liquid thickness is the detrimental effect on resolution capability [92]. In general, resolution improves as the liquid thickness decreases. Still, resolutions from ~ 10 nm onwards are easily achievable. Imaging at thin electrolyte conditions is therefore achieved by reducing the liquid thickness with introduced bubbles formed radiolytically [89, 93], or electrochemically [32]. Figure 4a shows a workflow using this approach to study Pt on carbon degradation by applying an AST protocol. The electrochemistry was measured under thick electrolyte conditions, and to record images, bubbles were introduced to reduce the liquid thickness. Although resolution tends to improve, it is safe to assume that bubbles, independent of their origin, will create new concentration and temperature gradients, creating a chemical environment that would drastically alter the surface of the electrode/material studied [48, 94, 95]. Furthermore, if the bubbles cannot be flushed away after imaging, initial conditions with fresh electrolyte are not secured, and might also influence other factors like ohmic resistances.

Several EC-LP-EM studies, besides the ones in Fig. 4, apply other EM techniques to characterize the materials before, during, or after electrochemical protocols. Some use electron energy loss spectroscopy (EELS) [91, 96, 97], energy dispersive X-ray spectroscopy (EDX) [65, 66, 73, 74, 77, 97], and electron diffraction (ED). Whether it is selected area [65, 98, 99], cryogenic approaches with scanning electron nano beam diffraction [89], or with 4D-STEM [97, 100]. The electrochemical results obtained with these techniques cannot rule out radiation artifacts; however, they still collect valuable data for *in situ* characterization of materials. Furthermore, in the case of ED techniques, its benefit relies on the ability to translate time-resolved diffraction patterns into structural changes of electrocatalysts with a lower dose than their imaging counterparts. Still, liquid thickness needs to be carefully controlled to obtain meaningful patterns.

Another way to identify beam effects was achieved via gas chromatography mass spectroscopy (GC–MS) batch analyses by directly analyzing the exhaust electrolyte obtained after applying electrochemical protocols and applying only irradiation *in situ* (Fig. 4b) [66]. By investigating degradation mechanisms of a Na-Ion battery anode *in situ* vs. *ex situ*, the results showed similar structural changes attributed to the same degradation routes. However, the *in situ* experiments showed thicker solid electrolyte interphases than *ex situ*. Still, the results only under irradiation showed no electrolyte degradation products, thus attributing the degradation *in situ* to electrochemistry. Lastly, Fig. 4c shows the results of a study of Cu cubes degradation during electrochemical nitrate reduction using several methods, including *operando:* transmission X-ray microscopy, X-ray absorption spectroscopy, and Raman spectroscopy. The *in situ* and *operando* results were compared to *ex situ* experiments, as well as

non-beam experiments, where the results concluded on similar degradation mechanisms. However, the study reported that the constant vs. intermittent irradiation case under extended periods of time indeed led to an accelerated degradation of the Cu_2O cubes [64]. The combination of these *in situ* and *operando* techniques for materials characterization during reaction conditions cannot identify beam effects but proves to be promising since these techniques resolve changes in the surface chemistry of electrode materials during electrochemical reactions on different levels. EC-LP-EM on a specific imaged area, whereas the synchrotron of an assembly of electrocatalysts [64].

As shown above, reliable electrochemistry can be achieved when studying different electrocatalysts or electrode materials for different electrochemical systems under careful experimental design. Correlating EC-LP-EM results with bulk experiments and with *in situ* non-irradiated results, as well as prior knowledge of radiation chemistry obtained from simulations, is still necessary to give a broad idea of the trends to then draw conclusions for real device scenarios. Still, the studies described have enabled the live observation of these highly dynamic processes.

Conclusions and outlook

With this snapshot review, we summarize recent developments in EC-LP-EM and how electrode architecture, radiation chemistry, and the microscope environment can affect electrochemical reactions. We acknowledge that the complexity of experimental design, data collection, and their interpretation are bottlenecks that still prevent LP-EM from having a higher scientific throughput. Nevertheless, under careful consideration, EC-LP-EM studies show incredible potential in directly observing dynamic processes at the nanoscale, with great chances to resolve open challenges of dynamic processes at solid–liquid interfaces. Besides, we propose harnessing radiolysis in studies where the effect of extreme conditions over time is of central importance. Thus, EC-LP-EM experiments with the inevitable artifacts from radiolysis can be deliberately tailored to accelerate stress testing significantly. Hence, allowing the understanding of degradation mechanisms of different catalytic materials for faster screening of materials, with the final goal of aiding the transition towards green renewable energies. Still, to achieve this, a clear understanding of all the parasitic reactions coming from radiolysis, besides the ones expected from electrochemistry, is fundamental to better identify, distinguish, and explain the different live imaged physico-chemical processes.

Acknowledgements The authors thank Dr. Stefan Merkens for providing display items concerning electrode architectures and valuable suggestions during the final editing. Also, we thank Angelina Cuomo for valuable electrochemical discussions.

Author contributions A. Lucía Morales: Conceptualization, Data curation, Investigation, Visualization, Writing—original draft. Andreas Körner: Conceptualization, Writing—review & editing. Birk Fritsch: Conceptualization, Resources, Writing—review & editing. Serhiy Cherevko: Resources, Writing—review & editing. Giuseppe De Salvo: Visualization, Writing—review & editing. Karl J. J. Mayrhofer: Writing—review & editing. Andreas Hutzler: Conceptualization, Project administration, Resources, Supervision, Writing—review & editing.

Funding Open Access funding enabled and organized by Projekt DEAL. No funding was received to assist with the preparation of this manuscript.

Data availability Not applicable.

Declarations

Conflict of interest The authors declare no conflict of interest.

References

1. P. Kurzweil, HISTORY | electrochemical capacitors. Encycl. Electrochem. Power Sources (2009). https://doi.org/10.1016/B978-044452745-5.00006-X
2. European Synchrotron Radiation Facility (ESRF): ESRD Highlights 2024 (2024)
3. Y. Yang, J. Feijóo, V. Briega-Martos, Q. Li, M. Krumov, S. Merkens, G. de Salvo, A. Chuvilin, J. Jin, H. Huang, C.J. Pollock, M.B. Salmeron, C. Wang, D.A. Muller, H.D. Abruña, P. Yang, Operando methods: a new era of electrochemistry. Curr. Opin. Electrochem. (2023). https://doi.org/10.1016/j.coelec.2023.101403
4. J. Weiss, Radiochemistry of aqueous solutions. Nature (1944). https://doi.org/10.1038/153748a0
5. J. Weiss, Primary processes in the action of ionizing radiations on water: formation and reactivity of self-trapped electrons ('Polarons'). Nature (1960). https://doi.org/10.1038/186751a0
6. M. Spotheim-Maurizot, et al., Radiation Chemistry: From Basics to Applications in Material and Life Sciences. EDP Sciences. (2008)
7. N.M. Schneider, Electron Beam Effects in Liquid Cell TEM and STEM. In: Ross, F.M. (ed.) Liquid Cell Electron Microscopy, Cambridge University Press (2016)

8. B. Fritsch, S. Lee, A. Körner, N.M. Schneider, F.M. Ross, A. Hutzler, The influence of ionizing radiation on quantification for in situ and operando liquid-phase electron microscopy. Adv. Mater. (2025). https://doi.org/10.1002/adma.202415728
9. J. Drnec, S. Lyonnard, Battery research needs more reliable, representative and reproducible synchrotron characterizations. Nat. Nanotechnol. (2025). https://doi.org/10.1038/s41565-025-01921-4
10. C. Villevieille, The challenge of studying interfaces in battery materials. Nat. Nanotechnol. (2025). https://doi.org/10.1038/s41565-024-01836-6
11. S. Cherevko, K. Mayrhofer, *On-line inductively coupled plasma spectrometry in electrochemistry: basic principles and applications* (Encyclopedia of Interfacial Chemistry, Elsevier, 2018)
12. O. Kasian, S. Geiger, K.J.J. Mayrhofer, S. Cherevko, Electrochemical on-line ICP-MS in electrocatalysis research. Chem. Rec. (2019). https://doi.org/10.1002/tcr.201800162
13. K.J. Mayrhofer, J.C. Meier, S.J. Ashton, G.K. Wiberg, F. Kraus, M. Hanzlik, M. Arenz, Fuel cell catalyst degradation on the nanoscale. Electrochem. Commun. (2008). https://doi.org/10.1016/j.elecom.2008.05.032
14. A.R. Kamšek, F. Ruiz-Zepeda, M. Bele, A. Logar, G. Dražić, N. Hodnik, Structure-stability relationships in Pt-alloy nanoparticles using identical-location four-dimensional scanning transmission electron microscopy and unsupervised machine learning. ACS Nano (2025). https://doi.org/10.1021/acsnano.4c12528
15. N. de Jonge, F.M. Ross, Electron microscopy of specimens in liquid. Nat. Nanotechnol. (2011). https://doi.org/10.1038/nnano.2011.161
16. F.M. Ross, Opportunities and challenges in liquid cell electron microscopy. Science (New York, NY) (2015). https://doi.org/10.1126/science.aaa9886
17. N.M. Schneider, M.M. Norton, B.J. Mendel, J.M. Grogan, F.M. Ross, H.H. Bau, Electron-water interactions and implications for liquid cell electron microscopy. J. Phys. Chem. C (2014). https://doi.org/10.1021/jp507400n
18. B. Fritsch, T.S. Zech, M.P. Bruns, A. Körner, S. Khadivianazar, M. Wu, N. Zargar Talebi, S. Virtanen, T. Unruh, M.P.M. Jank, E. Spiecker, A. Hutzler, Radiolysis-driven evolution of gold nanostructures - model verification by scale bridging in situ liquid-phase transmission electron microscopy and X-ray diffraction. Adv. Sci. (2022). https://doi.org/10.1002/advs.202202803
19. S. Merkens, C. Tollan, G. de Salvo, K. Bejtka, M. Fontana, A. Chiodoni, J. Kruse, M.A. Iriarte-Alonso, M. Grzelczak, A. Seifert, A. Chuvilin, Toward sub-second solution exchange dynamics in flow reactors for liquid-phase transmission electron microscopy. Nat. Commun. (2024). https://doi.org/10.1038/s41467-024-46842-3
20. S. Merkens, G. Salvo, A. Chuvilin, The effect of flow on radiolysis in liquid phase-TEM flow cells. Nano Ex. (2022). https://doi.org/10.1088/2632-959X/acad18
21. D. Cheng, J. Hong, D. Lee, S.-Y. Lee, H. Zheng, In situ TEM characterization of battery materials. Chem. Rev. (2025). https://doi.org/10.1021/acs.chemrev.4c00507
22. M.A. Smeaton, P. Abellan, S.R. Spurgeon, R.R. Unocic, K.L. Jungjohann, Tutorial on in situ and operando (scanning) transmission electron microscopy for analysis of nanoscale structure-property relationships. ACS Nano (2024). https://doi.org/10.1021/acsnano.4c09256
23. A. Körner, B. Fritsch, A.L. Morales, P. Malgaretti, A. Hutzler, Panta Rhei - tuning silver nanostructure evolution with flow and radiolysis in liquid phase STEM. Nano Today (2025). https://doi.org/10.1016/j.nantod.2024.102575
24. B.K. Troudt, C.R. Rousseau, X.I.N. Dong, E.L. Anderson, P. Bühlmann, Recent progress in the development of improved reference electrodes for electrochemistry. Anal. Sci. (2022). https://doi.org/10.2116/analsci.21SAR11
25. S. Choudhary, K. Marusak, T. Eldred, R.G. Kelly, Use of a bipolar, metallic Luggin-Haber probe for electrochemical measurements of interfacial potential. J. Electrochem. Soc. (2022). https://doi.org/10.1149/1945-7111/aca367
26. P. Grosse, A. Yoon, C. Rettenmaier, A. Herzog, S.W. Chee, B. Roldan Cuenya, Dynamic transformation of cubic copper catalysts during CO2 electroreduction and its impact on catalytic selectivity. Nat. Commun. (2021). https://doi.org/10.1038/s41467-021-26743-5
27. COMSOL: Electrodeposition Module Application Library: Secondary Current Distribution in a Zinc Electrowinning Cell. Application ID: 10188 (2015–2024)
28. COMSOL: Electrochemistry Module Application Library: Wire Electrode. Application ID: 3471 (2015–2024)
29. T. Pérez, C. Ponce de León, F.C. Walsh, J.L. Nava, Simulation of current distribution along a planar electrode under turbulent flow conditions in a laboratory filter-press flow cell. Electrochim. Acta (2015). https://doi.org/10.1016/j.electacta.2014.11.166
30. R.M. Wittman, R.L. Sacci, R. Unocic, T. Zawodzinski, In situ liquid electron microscope cells strongly attenuate electrochemical behavior. J. Electrochem. Soc. (2024). https://doi.org/10.1149/1945-7111/ad963a
31. X. Wei, M. Noyong, U. Simon, Advanced electrode design enables homogeneous electric field distribution for metal deposition studies via in situ liquid cell TEM. iScience (2024). https://doi.org/10.1016/j.isci.2024.111119
32. S. Kim, J. Kwag, M. Lee, S. Kang, D. Kim, J.-G. Oh, Y.-J. Heo, J. Ryu, J. Park, Unraveling serial degradation pathways of supported catalysts through reliable electrochemical liquid-cell TEM analysis. J. Am. Chem. Soc. (2025). https://doi.org/10.1021/jacs.4c08825
33. S. Lee, S.F. Tan, F.M. Ross, Electrochemical Transmission Electron Microscopy (EC-TEM) of capacitance-induced electrodeposition and coarsening on graphene. Microsc. Microanal. (2024). https://doi.org/10.1093/mam/ozae044.814
34. Y. Wang, D. Rastogi, K. Malek, J. Sun, A. Asa-Awuku, T.J. Woehl, Electric field-induced water condensation visualized by vapor-phase transmission electron microscopy. J. Phys. Chem. A (2023). https://doi.org/10.1021/acs.jpca.2c08187
35. C. Liu, A.J. Bard, Electrostatic electrochemistry at insulators. Nat. Mater. (2008). https://doi.org/10.1038/nmat2160
36. X. Wang, Q. Yang, S. Singh, H. Borrmann, V. Hasse, C. Yi, Y. Li, M. Schmidt, X. Li, G.H. Fecher, D. Zhou, B. Yan, C. Felser, Topological semimetals with intrinsic chirality as spin-controlling electrocatalysts for the oxygen evolution reaction. Nat. Energy (2025). https://doi.org/10.1038/s41560-024-01674-9
37. A. Giner-Requena, J. Gracia, T. Lana-Villarreal, R. Gómez, Magnetic Effects in electrocatalysis studied with electrochemical impedance spectroscopy: the cases of oxygen reduction and evolution reactions on cobalt ferrite electrodes. Chemsuschem (2024). https://doi.org/10.1002/cssc.202402167
38. Y. Zhang, P. Guo, S. Li, J. Sun, W. Wang, B. Song, X. Yang, X. Wang, Z. Jiang, G. Wu, P. Xu, Magnetic field assisted electrocatalytic oxygen evolution reaction of nickel-based materials. J. Mater. Chem. A (2022). https://doi.org/10.1039/D1TA09444K
39. F.A. Garcés-Pineda, M. Blasco-Ahicart, D. Nieto-Castro, N. López, J.R. Galán-Mascarós, Direct magnetic enhancement of electrocatalytic water oxidation in alkaline media. Nat. Energy (2019). https://doi.org/10.1038/s41560-019-0404-4
40. S. Cherevko, Electron spin matters. Nat. Energy (2025). https://doi.org/10.1038/s41560-024-01697-2
41. A.J. Bard, L.R. Faulkner, H.S. White, *Electrochemical methods fundamentals and applications* (John Wiley & Sons, 2001)

42. D.A. Armstrong, R.E. Huie, W.H. Koppenol, S.V. Lymar, G. Merényi, P. Neta, B. Ruscic, D.M. Stanbury, S. Steenken, P. Wardman, Standard electrode potentials involving radicals in aqueous solution: inorganic radicals (IUPAC technical report). Pure Appl. Chem. (2015). https://doi.org/10.1515/pac-2014-0502
43. J. Lee, D. Nicholls, N.D. Browning, B.L. Mehdi, Controlling radiolysis chemistry on the nanoscale in liquid cell scanning transmission electron microscopy. Phys. Chem. Chem. Phys. (2021). https://doi.org/10.1039/d0cp06369j
44. G. Inzelt, Crossing the bridge between thermodynamics and electrochemistry. From the potential of the cell reaction to the electrode potential. ChemTexts (2015). https://doi.org/10.1007/s40828-014-0002-9
45. G. Jerkiewicz, Standard and reversible hydrogen electrodes: theory, design, operation, and applications. ACS Catal. (2020). https://doi.org/10.1021/acscatal.0c02046
46. D. Gray, A. Cahill, Theoretical analysis of mixed potentials. J. Electrochem. Soc. (1969). https://doi.org/10.1149/1.2411894
47. J.M. Grogan, N.M. Schneider, F.M. Ross, H.H. Bau, Bubble and pattern formation in liquid induced by an electron beam. Nano Lett. (2014). https://doi.org/10.1021/nl404169a
48. B. Fritsch, A. Hutzler, M. Wu, S. Khadivianazar, L. Vogl, M.P.M. Jank, M. März, E. Spiecker, Accessing local electron-beam induced temperature changes during in situ liquid-phase transmission electron microscopy. Nanoscale Adv. (2021). https://doi.org/10.1039/d0na01027h
49. J. Priesner, T. Kraus, N. de Jonge, Nanoscale writing of gold nanoparticle assemblies at the liquid-vapor interface using a focused electron beam. Adv. Mater. Interfaces (2022). https://doi.org/10.1002/admi.202200699
50. C. Koenig, A.B.S. Da Fanta, J.R. Jinschek, Measurement of electron beam induced sample heating in SEM experiments. Ultramicroscopy (2025). https://doi.org/10.1016/j.ultramic.2025.114195
51. S. Lee, N.M. Schneider, S.F. Tan, F.M. Ross, Temperature dependent nanochemistry and growth kinetics using liquid cell transmission electron microscopy. ACS Nano (2023). https://doi.org/10.1021/acsnano.2c11477
52. Z. Ding, Y. Tang, V.S.K. Chakravadhanula, Q. Ma, F. Tietz, Y. Dai, T. Scherer, C. Kübel, Exploring the influence of focused ion beam processing and scanning electron microscopy imaging on solid-state electrolytes. Microscopy (2023). https://doi.org/10.1093/jmicro/dfac064
53. R.E. Robberstad Møller-Nilsen, S. Canepa, E. Jensen, H. Sun, I.A. Moreno-Hernandez, M.N. Yesibolati, A.P. Alivisatos, K.S. Mølhave, Quantifying aqueous radiolytic products in liquid phase electron microscopy. J. Phys. Chem. C (2023). https://doi.org/10.1021/acs.jpcc.3c02359
54. B. Fritsch, A. Körner, T. Couasnon, R. Blukis, M. Taherkhani, L.G. Benning, M.P.M. Jank, E. Spiecker, A. Hutzler, Tailoring the acidity of liquid media with ionizing radiation: rethinking the acid-base correlation beyond pH. J. Phys. Chem. Lett. (2023). https://doi.org/10.1021/acs.jpclett.3c00593
55. A. Korber, F.E. Furcas, M. Pundir, D.S. Kammer, U.M. Angst, PourPy - A python package to generate potential-pH diagrams. JOSS (2024). https://doi.org/10.21105/joss.06536
56. M. Pourbaix: Atlas of Electrochemical Equilibria in Aqueous Solutions. NACE (1974)
57. G.V. Buxton, R.M. Sellers, The radiation chemistry of metal ions in aqueous solution. Coord. Chem. Rev. (1977). https://doi.org/10.1016/S0010-8545(00)80328-8
58. A.A. Topalov, S. Cherevko, A.R. Zeradjanin, J.C. Meier, I. Katsounaros, K.J.J. Mayrhofer, Towards a comprehensive understanding of platinum dissolution in acidic media. Chem. Sci. (2014). https://doi.org/10.1039/C3SC52411F
59. S. Cherevko, A.R. Zeradjanin, G.P. Keeley, K.J.J. Mayrhofer, A comparative study on gold and platinum dissolution in acidic and alkaline media. J. Electrochem. Soc. (2014). https://doi.org/10.1149/2.0881412jes
60. V. Briega-Martos, K. Stojanovski, M. Zlatar, C. Göllner, S. Cherevko, pH dependence of noble metals dissolution: platinum. Electrochim. Acta (2024). https://doi.org/10.1016/j.electacta.2024.144793
61. Z. Wu, G. Yang, Q. Zhang, Z. Liu, F. Peng, Deciphering the high overpotential of the oxygen reduction reaction via comprehensively elucidating the open circuit potential. Energy Environ. Sci. (2024). https://doi.org/10.1039/D3EE04368A
62. Y. Yokoyama, T. Fukutsuka, K. Miyazaki, T. Abe, Origin of the electrochemical stability of aqueous concentrated electrolyte solutions. J. Electrochem. Soc. (2018). https://doi.org/10.1149/2.0491814jes
63. V. Briega-Martos, T. Fuchs, J. Drnec, O.M. Magnussen, S. Cherevko, Effects of anions and surface structure on Pt single crystal dissolution in acidic electrolytes. ChemElectroChem (2024). https://doi.org/10.1002/celc.202300554
64. A. Yoon, L. Bai, F. Yang, F. Franco, C. Zhan, M. Rüscher, J. Timoshenko, C. Pratsch, S. Werner, H.S. Jeon, MCd.O. Monteiro, S.W. Chee, B. Roldan Cuenya, Revealing catalyst restructuring and composition during nitrate electroreduction through correlated operando microscopy and spectroscopy. Nat. Mater. (2025). https://doi.org/10.1038/s41563-024-02084-8
65. N. Ortiz Peña, D. Ihiawakrim, M. Han, B. Lassalle-Kaiser, S. Carenco, C. Sanchez, C. Laberty-Robert, D. Portehault, O. Ersen, Morphological and structural evolution of Co3O4 nanoparticles revealed by in situ electrochemical transmission electron microscopy during electrocatalytic water oxidation. ACS Nano (2019). https://doi.org/10.1021/acsnano.9b04745
66. K. Gallegos-Moncayo, N. Folastre, M. Toledo, H. Tonnoir, F. Rabuel, G. Gachot, Da. Huo, A. Demortière, Coupling liquid electrochemical TEM and Mass-spectrometry to investigate electrochemical reactions occurring in a na-ion battery anode. Small Methods (2024). https://doi.org/10.1002/smtd.202400365
67. F. Shi, F. Li, Y. Ma, F. Zheng, R. Feng, C. Song, P. Tao, W. Shang, T. Deng, J. Wu, In situ transmission electron microscopy study of nanocrystal formation for electrocatalysis. ChemNanoMat (2019). https://doi.org/10.1002/cnma.201900497
68. W. Dachraoui, T.R. Henninen, D. Keller, R. Erni, Multi-step atomic mechanism of platinum nanocrystals nucleation and growth revealed by in-situ liquid cell STEM. Sci. Rep. (2021). https://doi.org/10.1038/s41598-021-03455-w
69. J. Sun, B. Fritsch, A. Körner, M. Taherkhani, C. Park, M. Wang, A. Hutzler, T.J. Woehl, Discovery of molecular intermediates and nonclassical nanoparticle formation mechanisms by liquid phase electron microscopy and reaction throughput analysis. Small Struct. (2024). https://doi.org/10.1002/sstr.202400146
70. A. Hutzler, T. Schmutzler, M.P.M. Jank, R. Branscheid, T. Unruh, E. Spiecker, L. Frey, Unravelling the mechanisms of gold-silver core-shell nanostructure formation by in situ TEM using an advanced liquid cell design. Nano Lett. (2018). https://doi.org/10.1021/acs.nanolett.8b03388
71. A. Hutzler, B. Fritsch, M.P.M. Jank, R. Branscheid, R.C. Martens, E. Spiecker, M. März, In situ liquid cell TEM studies on etching and growth mechanisms of gold nanoparticles at a solid–liquid–gas interface. Adv. Mater. Interfaces (2019). https://doi.org/10.1002/admi.201901027
72. E. Sutter, K. Jungjohann, S. Bliznakov, A. Courty, E. Maisonhaute, S. Tenney, P. Sutter, In situ liquid-cell electron microscopy of silver-palladium galvanic replacement reactions on silver nanoparticles. Nat. Commun. (2014). https://doi.org/10.1038/ncomms5946
73. S.F. Tan, G. Lin, M. Bosman, U. Mirsaidov, C.A. Nijhuis, Real-time dynamics of galvanic replacement reactions of Silver

nanocubes and Au studied by liquid-cell transmission electron microscopy. ACS Nano (2016). https://doi.org/10.1021/acsnano.6b03020
74. E.A. Sutter, P.W. Sutter, In situ liquid cell electron microscopy of Ag-Au galvanic replacement reactions. Nanoscale (2017). https://doi.org/10.1039/c6nr07293c
75. S.W. Chee, S.F. Tan, Z. Baraissov, M. Bosman, U. Mirsaidov, Direct observation of the nanoscale Kirkendall effect during galvanic replacement reactions. Nat. Commun. (2017). https://doi.org/10.1038/s41467-017-01175-2
76. J.S. Du, K. He, Y. Xu, C.B. Wahl, D.D. Xu, V.P. Dravid, C.A. Mirkin, Galvanic transformation dynamics in heterostructured nanoparticles. Adv. Funct. Mater. (2021). https://doi.org/10.1002/adfm.202105866
77. W. Wang, I. Erofeev, Y. He, F. Yang, H. Yan, J. Lu, U. Mirsaidov, Direct observation of hollow bimetallic nanoparticle formation through galvanic replacement and etching reactions. Nano Lett. (2023). https://doi.org/10.1021/acs.nanolett.3c02575
78. B. Fritsch, P. Malgaretti, J. Harting, K.J.J. Mayrhofer, A. Hutzler, Precision of radiation chemistry networks: playing Jenga with kinetic models for liquid-phase electron microscopy. Precis. Chem. (2023). https://doi.org/10.1021/prechem.3c00078
79. H. Wu, H. Sun, R.A.J.F. Oerlemans, S. Li, J. Shao, J. Wang, R.R.M. Joosten, X. Lou, Y. Luo, H. Zheng, L.K.E.A. Abdelmohsen, H.H.P. Garza, J.C.M. van Hest, H. Friedrich, Understanding, mimicking, and mitigating radiolytic damage to polymers in liquid phase transmission electron microscopy. Adv. Mater. (2024). https://doi.org/10.1002/adma.202402987
80. J. Korpanty, L.R. Parent, N.C. Gianneschi, Enhancing and mitigating radiolytic damage to soft matter in aqueous phase liquid-cell transmission electron microscopy in the presence of gold nanoparticle sensitizers or isopropanol scavengers. Nano Lett. (2021). https://doi.org/10.1021/acs.nanolett.0c04636
81. I.A. Moreno-Hernandez, M.F. Crook, J.C. Ondry, A.P. Alivisatos, Redox mediated control of electrochemical potential in liquid cell electron microscopy. J. Am. Chem. Soc. (2021). https://doi.org/10.1021/jacs.1c03906
82. M. Fratarcangeli, S.A. Vigil, I.A. Moreno-Hernandez, Understanding electrochemical degradation via liquid phase transmission electron microscopy. J. Phys. Chem. C (2025). https://doi.org/10.1021/acs.jpcc.5c01320
83. M. Fratarcangeli, S.A. Vigil, Z. Lin, C.J. Soderstedt, I.A. Moreno-Hernandez, Direct observation of structural disorder effects on iridium dioxide nanocrystal dissolution. Matter (2025). https://doi.org/10.1016/j.matt.2024.11.003
84. P. Abellan, B.L. Mehdi, L.R. Parent, M. Gu, C. Park, W. Xu, Y. Zhang, I. Arslan, J.-G. Zhang, C.-M. Wang, J.E. Evans, N.D. Browning, Probing the degradation mechanisms in electrolyte solutions for Li-ion batteries by in situ transmission electron microscopy. Nano Lett. (2014). https://doi.org/10.1021/nl404271k
85. D. Ortiz, V. Steinmetz, D. Durand, S. Legand, V. Dauvois, P. Maître, S. Le Caër, Radiolysis as a solution for accelerated ageing studies of electrolytes in Lithium-ion batteries. Nat. Commun. (2015). https://doi.org/10.1038/ncomms7950
86. B. Fritsch, Quantification of Electron Beam-induced Effects in Liquid-phase Transmission Electron Microscopy. Friedrich-Alexander-Universität Erlangen-Nürnberg (FAU) (2023).
87. G. De Salvo, S. Merkens, A. Körner, B. Fritsch, P. Malgaretti, A. Hutzler, A. Chuvilin, A workflow for modeling radiolysis in chemically, physically, and geometrically complex scenarios. iScience (2025). https://doi.org/10.1016/j.isci.2025.112374
88. R.F. Egerton, P. Li, M. Malac, Radiation damage in the TEM and SEM. Micron (2004). https://doi.org/10.1016/j.micron.2004.02.003
89. H. Koh, S. Das, Y. Zhang, E. Detsi, E.A. Stach, Electron beam-induced artifacts in SEI characterization: evidence from controlled-dose diffraction studies. ACS Energy Lett. (2025). https://doi.org/10.1021/acsenergylett.4c03337
90. R.F. Egerton, Dose measurement in the TEM and STEM. Ultramicroscopy (2021). https://doi.org/10.1016/j.ultramic.2021.113363
91. M.E. Holtz, Y. Yu, D. Gunceler, J. Gao, R. Sundararaman, K.A. Schwarz, T.A. Arias, H.D. Abruña, D.A. Muller, Nanoscale imaging of lithium ion distribution during in situ operation of battery electrode and electrolyte. Nano Lett. (2014). https://doi.org/10.1021/nl404577c
92. N. de Jonge, L. Houben, R.E. Dunin-Borkowski, F.M. Ross, Resolution and aberration correction in liquid cell transmission electron microscopy. Nat. Rev. Mater. (2019). https://doi.org/10.1038/s41578-018-0071-2
93. A. Impagnatiello, C.F. Cerqueira, P.-E. Coulon, A. Morin, S. Escribano, L. Guetaz, M.-C. Clochard, G. Rizza, Degradation mechanisms of supported Pt nanocatalysts in proton exchange membrane fuel cells: an operando study through liquid cell transmission electron microscopy. ACS Appl. Energy Mater. (2020). https://doi.org/10.1021/acsaem.9b02000
94. Z.-W. Yin, S.B. Betzler, T. Sheng, Q. Zhang, X. Peng, J. Shangguan, K.C. Bustillo, J.-T. Li, S.-G. Sun, H. Zheng, Visualization of facet-dependent pseudo-photocatalytic behavior of TiO2 nanorods for water splitting using in situ liquid cell TEM. Nano Energy (2019). https://doi.org/10.1016/j.nanoen.2019.05.068
95. L. Zhang, R. Iwata, Z. Lu, X. Wang, C.D. Díaz-Marín, Y. Zhong, Bridging innovations of phase change heat transfer to electrochemical gas evolution reactions. Chem. Rev. (2024). https://doi.org/10.1021/acs.chemrev.4c00157
96. T.-H. Shen, L. Spillane, J. Peng, Y. Shao-Horn, V. Tileli, Switchable wetting of oxygen-evolving oxide catalysts. Nat. Catal. (2022). https://doi.org/10.1038/s41929-021-00723-w
97. Z. Ding, Y. Tang, T. Ortmann, J.K. Eckhardt, Y. Dai, M. Rohnke, G. Melinte, C. Heiliger, J. Janek, C. Kübel, The impact of microstructure on filament growth at the sodium metal anode in all-solid-state sodium batteries. Adv. Energy Mater. (2023). https://doi.org/10.1002/aenm.202302322
98. A.M. Abdellah, F. Ismail, O.W. Siig, J. Yang, C.M. Andrei, L.-A. DiCecco, A. Rakhsha, K.E. Salem, K. Grandfield, N. Bassim, R. Black, G. Kastlunger, L. Soleymani, D. Higgins, Impact of palladium/palladium hydride conversion on electrochemical CO2 reduction via in-situ transmission electron microscopy and diffraction. Nat. Commun. (2024). https://doi.org/10.1038/s41467-024-45096-3
99. W. Yu, S. Yue, M. Yang, M. Hashimoto, P. Liu, L. Zhu, W. Xie, T. Jones, M. Willinger, X. Huang, Operando TEM study of a working copper catalyst during ethylene oxidation. Nat. Commun. (2025). https://doi.org/10.1038/s41467-025-57418-0
100. Y. Yang, Y.-T. Shao, J. Jin, J. Feijóo, I. Roh, S. Louisia, S. Yu, M.V. Fonseca Guzman, C. Chen, D.A. Muller, H.D. Abruña, P. Yang, Operando electrochemical liquid-cell scanning transmission electron microscopy (EC-STEM) studies of evolving Cu nanocatalysts for CO 2 electroreduction. ACS Sustainable Chem. Eng. (2023). https://doi.org/10.1021/acssuschemeng.2c06542